Intrinsic Spin Hall Effect Induced by Quantum Phase Transition in HgCdTe Quantum Wells

Wen Yang and Kai Chang*

State Key Laboratory for Superlattices and Microstructures, Institute of Semiconductors, Chinese Academy of Sciences, P.O. Box 912, 100083, Beijing, China

Shou-Cheng Zhang

Department of Physics, McCullough Building, Stanford University, Stanford, California 94305-4045, USA

(Received 22 October 2007; published 6 February 2008)

The spin Hall effect can be induced by both extrinsic impurity scattering and intrinsic spin-orbit coupling in the electronic structure. The HgTe/CdTe quantum well has a quantum phase transition where the electronic structure changes from normal to inverted. We show that the intrinsic spin Hall effect of the conduction band vanishes on the normal side, while it is finite on the inverted side. By tuning the Cd content, the well width, or the bias electric field across the quantum well, the intrinsic spin Hall effect can be switched on or off and tuned into resonance under experimentally accessible conditions.

DOI: 10.1103/PhysRevLett.100.056602 PACS numbers: 72.25.−b, 71.70.Ej, 73.63.−b, 85.75.−d

Spin-polarized transport in nonmagnetic semiconductors is a crucial ingredient for realizing spintronic devices [1]. The spin Hall effect (SHE) opens up the promising prospect of generating spin currents in conventional semiconductors without applying an external magnetic field or introducing ferromagnetic elements. Recently the previously predicted extrinsic SHE (ESHE) [2] and the newly discovered intrinsic SHE (ISHE) [3] have become one of the most intensively studied subjects. The experimental observations of SHE have been reported by two groups [4,5] in n-type epilayers and two-dimensional electron and hole gases, although their theoretical interpretation as extrinsic or intrinsic is still ambiguous [6–8]. The ISHE in the 2D hole gas has no vertex correction [6], and its existence has been widely accepted [9]; the existence of the electron ISHE in two-dimensional systems is under substantial debate [10–17]. The current understanding is that the electron ISHE in the ideal model (single-band Hamiltonian with parabolic dispersion and linear Rashba and/or Dresselhaus spin splitting) is exactly canceled by the impurity induced vertex corrections in the clean limit [10,11], even for momentum dependent scattering [12–14].

Very recently quantum spin Hall effect was predicted theoretically and observed experimentally in a narrow gap HgTe quantum well with the unique inverted band structure [18]. The HgTe quantum well has a quantum phase transition when the quantum well thickness d is tuned across a critical thickness $d_c \approx 6$ nm. For $d < d_c$, the electronic structure is normal, similar to the GaAs quantum wells, where the conduction band has Γ_6 character, and the valence band Γ_8 character. In this regime, we show that the ISHE vanishes in the conduction band due to vertex corrections, consistent with previous results. For $d > d_c$, the electronic structure is inverted, where the conduction and the valence bands interchange their Γ_6-Γ_8 characters. In this regime, we show that the ISHE is finite in the conduction band. By varying the well width or the electric bias across the quantum well, the electron ISHE can be switched on or off or even tuned into resonance under experimentally accessible conditions.

First we develop a unified description of Γ_6-electron and Γ_8-hole SHE based on a general N-band effective-mass theory, which remains valid over the whole range of Γ_6-Γ_8 coupling strengths and band gaps. Following the new envelope function approach [19], the band-edge Bloch basis $\{\Phi_\mu\}$ is classified into N relevant bands $\{\Phi_j\}$ and infinite irrelevant bands $\{\Phi_l\}$. In the N-dimensional $\{\Phi_j\}$ subspace, the image of the Hamiltonian H for a general microstructure is $\mathbb{H}_{jj'} = \mathcal{H}_{jj'} + \sum_l \mathcal{H}_{jl}(E - E_l)^{-1}\mathcal{H}_{lj'}$ [19]. The image of an arbitrary operator O $(\neq H)$ can also be obtained as

$$\mathbb{O}_{jj'} = \mathcal{O}_{jj'} + \sum_l \left(\mathcal{O}_{jl} \frac{1}{E - E_l} \mathcal{H}_{lj'} + \mathcal{H}_{jl} \frac{1}{E - E_l} \mathcal{O}_{lj'} \right), \tag{1}$$

where $\mathcal{H}$ and $\mathcal{O}$ are, respectively, the image of H and O in the $\{\Phi_\mu\}$ space. Then the images of velocity $\mathbf{v}$, spin $\mathbf{s}$, and spin current $j_\alpha^\beta \equiv (v_\alpha s_\beta + s_\beta v_\alpha)/2 (\alpha, \beta = x, y, z)$ operators are given by $\vec{\mathbb{V}}_{jj'} = [\mathbf{r}, \mathbb{H}_{jj'}]/(i\hbar)$, $\vec{\mathbb{S}}_{jj'} = \langle \Phi_j | \mathbf{s} | \Phi_{j'} \rangle$, and $\mathbb{J}_\alpha^\beta = (\mathbb{V}_\alpha \mathbb{S}_\beta + \mathbb{S}_\beta \mathbb{V}_\alpha)/2$ [20]. With the Γ_6-Γ_8 coupling taken into account, they generalize the previous theories (which neglect this coupling) to the N-band case; e.g., the widely used single-band (four-band Luttinger-Kohn) model corresponds to $N = 2$ $(N = 4)$. We emphasize that explicit consideration of the Γ_6-Γ_8 coupling is important in determining electron ISHE, especially for strong Γ_6-Γ_8 coupled systems. Further, the different nonideal band structure factors [21,22] arise from the same origin (Γ_6-Γ_8 coupling), so they are not independent and should be incorporated self-consistently through explicit consideration of the Γ_6-Γ_8 coupling. We notice that

the equation-of-motion argument [13] (valid for $N = 2$) for the nonexistence of electron ISHE is not applicable to other values of N (e.g., $N = 4$, 6, or 8).

The above theory can be applied to study both ISHE and ESHE in a general microstructure. In the present work we consider ISHE only, due to its much larger magnitude compared to ESHE under typical conditions [7,8], especially for small electron density. The linear response spin Hall conductivity $\sigma_{\rm SH} = (e/\mathcal{A})\lim_{\omega\to 0}[G^z_{xy}(\omega) - G^z_{xy}(0)]/(i\omega)$, with $\mathcal{A}$ the sample area and $G^z_{xy}(\omega)$ the impurity-averaged retarded correlation function of $\mathbb{J}^z_y$ and $\mathbb{V}_x$. Using standard diagrammatic perturbation theory, $G^z_{xy}(\omega)$ is evaluated taking into account the impurity induced self-energy corrections in the self-consistent Born approximation and vertex corrections in the ladder approximation (inset of Fig. 1), yielding

$$\sigma_{\rm SH} = \frac{e}{\pi}\int_{-\infty}^{\infty} d\omega f(\omega) \lim_{\eta\to 0^+} {\rm Re}\Big[\frac{\partial P(\omega' + i\eta, \omega + i\eta)}{\partial \omega'} - \frac{\partial P(\omega' + i\eta, \omega - i\eta)}{\partial \omega'}\Big]_{\omega'=\omega},$$

where $f(\omega) = 1/[e^{(\hbar\omega-\mu)/(k_BT)} + 1]$, $P(z, z') = (1/\mathcal{A}){\rm Tr}\mathbb{J}^z_y \mathcal{G}(z)\Gamma(z, z')\mathcal{G}(z')$, $z = i\omega_m$, $z' = i\omega_n$, $\mathcal{G}_{ij}(z)$ and $\Gamma_{ij}(z, z')$ are, respectively, matrix elements of the impurity-averaged Matsubara Green's function and the dressed velocity vertex in the eigenstate basis of $\mathbb{H}$. They can be calculated from the Dyson equation and the vertex equation

$$\Gamma(z, z') = \mathbb{V}_x + n_I \int d\mathbf{R} \frac{\mathcal{U}(\mathbf{R})}{\hbar} \mathcal{G}(z)\Gamma(z, z')\mathcal{G}(z') \frac{\mathcal{U}(\mathbf{R})}{\hbar},$$

where n_I is the impurity concentration, and $\mathcal{U}_{ij}(\mathbf{R}) = \langle i|V_C(\mathbf{r} - \mathbf{R})|j\rangle$ is the matrix element of the single-impurity potential $V_C(\mathbf{r})$.

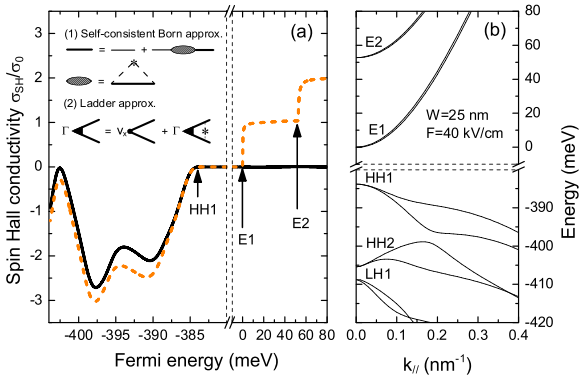

FIG. 1 (color online). (a) $\sigma_{\rm SH}$ for $W = 25$ nm and $F = 40$ kV/cm with (solid lines) or without (dashed lines) vertex corrections. Inset: (1) Dyson equation in the self-consistent Born approximation, and (2) vertex equation in the ladder approximation. (b) Corresponding energy spectrum.

Now we consider the lattice-matched symmetric $CdTe/Cd_xHg_{1-x}Te$ quantum well under electric bias. Its band gap can be tuned in a large range by varying the Cd content x, the well width W, or the bias electric field F. For such narrow gap systems, the $N = 8$ Kane model is a good starting point. It incorporates the aforementioned nonideal factors nonperturbatively and self-consistently. The Dresselhaus spin-orbit coupling is neglected because it is much smaller than the Rashba effect in a narrow gap quantum well [23], as verified by the quantitative agreement between theory and experiment in recent investigations on the transport properties of CdTe/HgTe quantum wells [24]. We also adopt the widely employed axial approximation (good for electrons and reasonable for holes in narrow gap systems) and short-range impurity potential $V_C(\mathbf{r}) = V_0\delta(\mathbf{r})$. All band parameters used in our numerical calculation are experimentally determined values [24,25]. We take the temperature $T = 0$ K and, unless specified, the effective disorder strength $\xi(\equiv n_I V_0^2) = 6.2$ eV^2 Å^3, corresponding to typical electron (hole) self-energy broadening 0.1 meV (1 meV) and collisional lifetime 6 ps (0.6 ps).

First we consider the weak Γ_6-Γ_8 coupling case $x = 0.37$ with $Eg(Hg_{0.63}Cd_{0.37}Te) \approx 0.4$ eV (Fig. 1). Without vertex corrections, the electron ISHE exhibits steplike increases [by approximately one universal value $\sigma_0 = e/(8\pi)$] at the edges of the first ($E1$) and second ($E2$) conduction bands. Such behavior is greatly suppressed by the inclusion of vertex corrections, in sharp contrast to the hole ISHE, which has an opposite sign and remains largely unaffected by vertex corrections. Therefore in the weak coupling regime, the results of the previous theories are recovered.

To explore electron ISHE in the strong coupling regime, we consider the CdTe/HgTe quantum well corresponding to $x = 0$. Because of the abnormal positions and effective masses of the Γ_6 electron and Γ_7 light-hole bands in the HgTe layer, the band gap E_g^Γ of the quantum well at $\mathbf{k}_\parallel = 0$ can be tuned by varying the well width or the electric bias. Figure 2(a) shows that the derivative of E_g^Γ is discontinuous at $W \approx 7$, 9, 24, and 28.5 nm, indicating certain phase transitions. Actually, the first critical point at $W \approx 7$ nm corresponds to the normal-inverted phase transition $E1$-HH1 $\rightarrow$ HH1-$E1$ [26]. Namely, the lowest conduction (highest valence) band changes from $E1$ to HH1 (HH1 to $E1$), where E (HH) denote Γ_6 electron (Γ_8 heavy-hole) states. Other critical points correspond to similar transitions [Fig. 2(b)]. They manifest the redshift (blueshift) of electron states $E2$, $E3$,...(heavy-hole states HH1, HH2,...) with increasing well width/electric bias due to weakening of the confinement/quantum-confined Stark effect. From Fig. 2(c), we see that in the $E1$-HH1 phase, $\sigma_{\rm SH}$ arising from the lowest conduction band ($E1$) is largely canceled by vertex corrections, especially for small Fermi energy. In contrast, in the HH1-$E1$ phase, the lowest conduction band

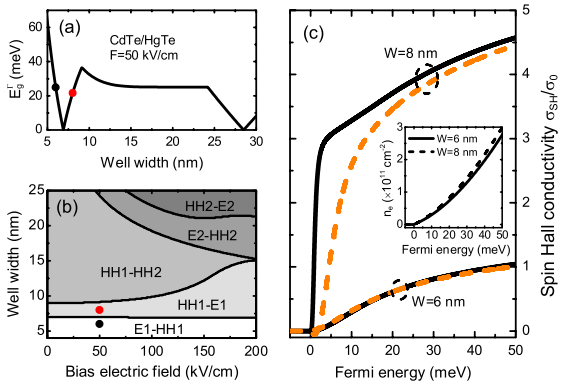

FIG. 2 (color online). (a) E_g^Γ for $F = 50$ kV/cm. (b) Band-edge ($\mathbf{k}_\parallel = 0$) phase diagram of the lowest conduction band and highest valence band. (c) σ_{SH} for $F = 50$ kV/cm, $W = 6$ and 8 nm, respectively [indicated by filled circles in (a) and (b)]. Solid (dashed) lines correspond to $\xi = 6.2(62)$ eV^2 Å^3. Inset: electron density vs Fermi energy.

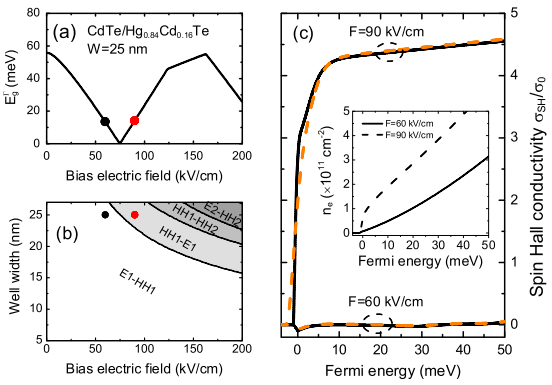

FIG. 3 (color online). (a) E_g^Γ for $W = 25$ nm. (b) Band-edge ($\mathbf{k}_\parallel = 0$) phase diagram of the lowest conduction band and highest valence band. (c) σ_{SH} for $W = 25$ nm, $F = 60$ and 90 kV/cm, respectively [indicated by filled circles in (a) and (b)]. Solid (dashed) lines correspond to $\xi = 6.2(62)$ eV^2 Å^3. Inset: electron density vs Fermi energy.

(HH1) takes on pure Γ_8 symmetry at small wave vectors, and its contribution to σ_{SH} is largely unaffected [27], leading to the abrupt increase of σ_{SH} accompanying the phase transition from $E1$-HH1 to HH1-$E1$. This phase transition induced ISHE is robust against impurity induced vertex corrections since it varies only slightly when ξ is increased by an order of magnitude, i.e., when typical electron lifetime [mobility] decreases from 6 to 0.6 ps [3×10^5 to 3×10^4 cm^2/(V s)]. By changing the well width, large electron ISHE can be switched on or off, especially for small Fermi energy or electron density [inset of Fig. 2(c)].

In the above, the phase transition occurs at small critical well width and the electric bias plays a minor role. When the critical well width increases, the bias electric field-induced quantum-confined Stark effect would become strong enough to induce the phase transition $E1$-HH1 $\rightarrow$ HH1-$E1$ and control the appearance of large electron ISHE. To demonstrate this, we consider the case $x = 0.16$ with Eg(Hg$_{0.84}$Cd$_{0.16}$Te) ≈ 0. For $W = 25$ nm, the band gap $E_g^\Gamma \approx 60$ meV at $F = 0$ and decreases to zero at $F \approx 75$ kV/cm [Fig. 3(a)]. The discontinuities of its derivative at $F \approx 75$, 1245, and 162 kV/cm clearly manifest the phase transitions plotted in Fig. 3(b). As a result, σ_{SH} in Fig. 3(c) shows a large increase when the bias electric field is tuned across the critical point. Again, the slight dependence on the disorder strength ξ manifests the robustness of the ISHE against impurity induced vertex corrections. The field-induced phase transition provides a dynamic way to switch on or off the electron ISHE, especially for small Fermi energy or electron density [inset of Fig. 3(c)].

Turning back to CdTe/HgTe quantum wells, Fig. 2(a) shows that the electric bias can induce the transition HH1 $\rightarrow$ $E2$ in the lowest conduction band or, equivalently, the transition $E2 \rightarrow$ HH1 in the second conduction band [Fig. 4(a)]. In the $E2$ phase, the Rashba spin splitting between the two branches of the second conduction band reverses its sign at a critical wave vector k_0 [Fig. 4(b)]. Analysis shows that this behavior comes from the coupling between the two branches and the interface states [28]; thus, it does not exist in the HH1 phase. By varying the well width or electric bias, such behavior can be switched on or off [Fig. 4(a)] and the critical wave vector [gray scale map in Fig. 4(a)] or critical electron density [inset of Fig. 4(c)] can be tuned, offering us the possibility to manipulate the ISHE arising from the second conduction band. Indeed, σ_{SH} in Fig. 4(c) exhibits a resonance when the Fermi energy coincides with the spin degeneracy point.

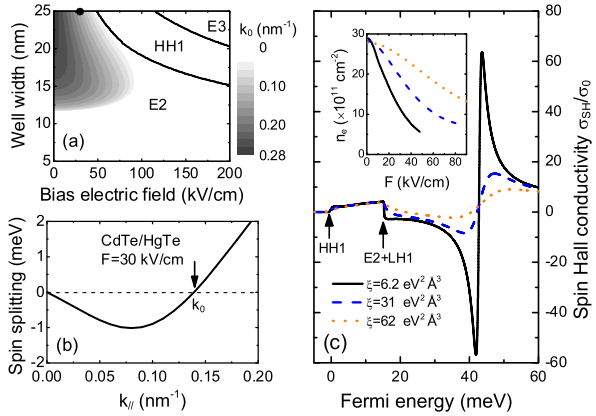

FIG. 4 (color online). (a) Band-edge ($\mathbf{k}_\parallel = 0$) phase diagram (the gray scale map in $E2$ phase indicates k_0) and (b) Rashba spin splitting (at $W = 25$ nm, $F = 30$ kV/cm) of the second conduction band. (c) σ_{SH} for $W = 25$ nm, $F = 30$ kV/cm [indicated by the filled circle in (a)] and different disorder strength ξ. Inset: critical electron density for $W = 25$ (solid line), 20 (dashed line), and 15 (dotted line) nm.

We notice that although such level-crossing induced resonance has been predicted for the widely accepted hole ISHE in p-type GaAs quantum wells (based on calculations that neglect vertex corrections) [29], a similar prediction for the much debated n-type systems still remains absent. For hole ISHE, a challenging hole lifetime $\gtrsim$10 ps or hole mobility $\mu_p \gtrsim 10^4$ cm^2/(V s) is required to observe the resonance [29]. For electron ISHE, the requirement is significantly relaxed to electron lifetime $\gtrsim$3 ps [corresponding to $\xi \lesssim 20$ eV^2 Å^3; cf. Fig. 4(c)] or electron mobility $\mu_n \gtrsim 2 \times 10^5$ cm^2/(V s). These have already been realized in previous experiments, e.g., $\mu_n = 3.2 \times 10^5$ cm^2/(V s) for $W = 7.8$ nm [30] and $\mu_n = 3.5 \times 10^5$ cm^2/(V s) for $W = 21$ nm [24] (close to the well width used in our calculation).

In summary, while the ISHE of the conduction band vanishes on the normal side of the Γ_6-Γ_8 phase transition in narrow gap HgCdTe quantum wells, a robust ISHE in the conduction band can be generated on the inverted side. By changing the Cd content, the well width, or the bias electric field, the ISHE can be switched on or off or tuned into resonance under experimentally accessible conditions. Reference [31] shows that the spin Hall effect can be experimentally observed by the nonlocal transport measurements in mesoscopic systems. We propose to carry out such measurement for both the normal and inverted quantum wells, both close to the transition. The difference uniquely singles out the ISHE contribution.

This work is supported by the NSFC Grant No. 60525405, the knowledge innovation project of CAS, the NSF under Grant No. DMR-0342832, and the U.S. Department of Energy, Office of Basic Energy Sciences under Contract No. DE-AC03-76SF00515.

*Corresponding author.
kchang@semi.ac.cn

[1] S. A. Wolf *et al.*, Science **294**, 1488 (2001).
[2] M. I. D'yakonov and V. I. Perel', Phys. Lett. **35A**, 459 (1971); J. E. Hirsch, Phys. Rev. Lett. **83**, 1834 (1999).
[3] S. Murakami, N. Nagaosa, and S. C. Zhang, Science **301**, 1348 (2003); J. Sinova *et al.*, Phys. Rev. Lett. **92**, 126603 (2004).
[4] Y. K. Kato, R. C. Myers, A. C. Gossard, and D. D. Awschalom, Science **306**, 1910 (2004); V. Sih *et al.*, Nature Phys. **1**, 31 (2005); V. Sih *et al.*, Phys. Rev. Lett. **97**, 096605 (2006); N. P. Stern *et al.*, Phys. Rev. Lett. **97**, 126603 (2006).
[5] J. Wunderlich, B. Kaestner, J. Sinova, and T. Jungwirth, Phys. Rev. Lett. **94**, 047204 (2005).
[6] B. A. Bernevig and S. C. Zhang, Phys. Rev. Lett. **95**, 016801 (2005).
[7] H. A. Engel, B. I. Halperin, and E. I. Rashba, Phys. Rev. Lett. **95**, 166605 (2005).
[8] W. K. Tse and S. Das Sarma, Phys. Rev. Lett. **96**, 056601 (2006).
[9] J. Sinova, S. Murakami, S. Q. Shen, and M. S. Choi, Solid State Commun. **138**, 214 (2006), and references therein.
[10] E. G. Mishchenko, A. V. Shytov, and B. I. Halperin, Phys. Rev. Lett. **93**, 226602 (2004); J. I. Inoue, G. E. W. Bauer, and L. W. Molenkamp, Phys. Rev. B **67**, 033104 (2003); **70**, 041303(R) (2004); D. N. Sheng, L. Sheng, Z. Y. Weng, and F. D. M. Haldane, *ibid.* **72**, 153307 (2005).
[11] K. Nomura, J. Sinova, N. A. Sinitsyn, and A. H. MacDonald, Phys. Rev. B **72**, 165316 (2005).
[12] E. I. Rashba, Phys. Rev. B **70**, 201309(R) (2004); R. Raimondi and P. Schwab, *ibid.* **71**, 033311 (2005).
[13] O. Chalaev and D. Loss, Phys. Rev. B **71**, 245318 (2005); O. V. Dimitrova, *ibid.* **71**, 245327 (2005).
[14] A. Khaetskii, Phys. Rev. Lett. **96**, 056602 (2006).
[15] A. G. Mal'shukov and K. A. Chao, Phys. Rev. B **71**, 121308(R) (2005); A. V. Shytov, E. G. Mishchenko, H. A. Engel, and B. I. Halperin, *ibid.* **73**, 075316 (2006); C. M. Wang, X. L. Lei, and S. Y. Liu, *ibid.* **73**, 113314 (2006); P. L. Krotkov and S. Das Sarma, *ibid.* **73**, 195307 (2006).
[16] İ. Adagideli and G. E. W. Bauer, Phys. Rev. Lett. **95**, 256602 (2005).
[17] L. Sheng, D. N. Sheng, and C. S. Ting, Phys. Rev. Lett. **94**, 016602 (2005); W. Ren *et al.*, *ibid.* **97**, 066603 (2006); Z. H. Qiao, W. Ren, J. Wang, and Hong Guo, *ibid.* **98**, 196402 (2007).
[18] B. A. Bernevig, T. L. Hughes, and S. C. Zhang, Science **314**, 1757 (2006); M. König *et al.*, Science **318**, 766 (2007).
[19] M. G. Burt, J. Phys. Condens. Matter **4**, 6651 (1992).
[20] In obtaining $\vec{\mathbb{S}}$ and $\mathbb{J}^{\beta}_{\alpha}$, we have neglected the second term in Eq. (1), which is smaller than the first term by a factor $\mathcal{H}_{jl}/(E - E_l) \ll 1$. This approximation becomes exact when $\{\Phi_j\}$ and $\{\Phi_l\}$ are chosen such that $\langle \Phi_j | \mathbf{s} | \Phi_l \rangle = 0$, e.g., for $N = 2$ (single-band model), 6 (six-band Luttinger-Kohn model), and 8 (Kane model).
[21] D. F. Nelson, R. C. Miller, and D. A. Kleinman, Phys. Rev. B **35**, 7770 (1987).
[22] W. Yang and K. Chang, Phys. Rev. B **73**, 113303 (2006); **74**, 193314 (2006).
[23] G. Lommer, F. Malcher, and U. Rössler, Phys. Rev. Lett. **60**, 728 (1988).
[24] X. C. Zhang *et al.*, Phys. Rev. B **63**, 245305 (2001); K. Ortner *et al.*, *ibid.* **66**, 075322 (2002).
[25] *II–VI and I–VII Compounds; Semimagnetic Compounds*, edited by U. Rössler, Landolt-Börnstein, Group III (Springer-Verlag, Berlin, 1999), Vol. 41B.
[26] N. F. Johnson, P. M. Hui, and H. Ehrenreich, Phys. Rev. Lett. **61**, 1993 (1988).
[27] Based on a modified single-band Rashba model instead of the correct heavy-hole Hamiltonian, the conclusion of Ref. [11] differs from ours. We believe that in the inverted band phase, single-band results should be taken cautiously due to the strong Γ_6-Γ_8 coupling.
[28] Y. R. Lin-Liu and L. J. Sham, Phys. Rev. B **32**, 5561 (1985).
[29] X. Dai, Z. Fang, Y. G. Yao, and F. C. Zhang, Phys. Rev. Lett. **96**, 086802 (2006).
[30] J. R. Meyer *et al.*, Phys. Rev. B **38**, 2204 (1988).
[31] E. M. Hankiewicz, L. W. Molenkamp, T. Jungwirth, and J. Sinova, Phys. Rev. B **70**, 241301(R) (2004).